

Title: **The Effect of Building Morphology on Sea Breeze Penetration over the Kanto Plain**

Authors: Taiki Sato, Taisei Corporation
Ryozo Ooka, University of Tokyo
Shuzo Murakami, Building Research Institute

Subject: Sustainability/Green/Energy

Keywords: CFD
Natural Ventilation
Renewable Energy

Publication Date: 2012

Original Publication: International Journal of High-Rise Buildings Volume 1 Number 2

Paper Type:

1. Book chapter/Part chapter
2. **Journal paper**
3. Conference proceeding
4. Unpublished conference paper
5. Magazine article
6. Unpublished

The Effect of Building Morphology on Sea Breeze Penetration over the Kanto Plain - Analysis of Mean Kinetic Energy Balance of Moving Control Volume along Sea Breeze -

Taiki Sato^{1†}, Ryoza Ooka² and Shuzo Murakami³

¹Taisei Corporation, Yokohama, 245-0051, Japan

²Institute of Industrial Science, The University of Tokyo, Tokyo, 153-8505, Japan

³Building Research Institute, Ibaraki, 305-0802, Japan

Abstract

In order to use sea breezes to counter the heat island phenomena, i.e. to promote urban ventilation, it is necessary to clarify the effect of building morphology and height on large-scale wind fields. In this study, the sea breeze in the vicinity of the Kanto Plain in Japan is simulated using a mesoscale meteorological model incorporating an urban canopy model, and the inland penetration of sea breezes is accurately reproduced. Additionally, a mean kinetic energy balance within a domain (Control Volume; CV) moving along the sea breeze is analysed. From the results, it is clarified that the sea breeze is interrupted by the resistance and turbulence caused by buildings at the centre of Tokyo. The interruption effect is increased in accordance with the height of these buildings. On the other hand, adverse pressure gradients interrupt in the internal region.

Keywords: Meteorological mesoscale model, Sea breeze, Moving control volume, Mean kinetic energy balance, Heat-island phenomenon

1. Introduction

The heat island phenomenon is observed in many cities (Taha, 1997; Inter-Ministry Coordination Committee to Mitigate Urban Heat Island 2004). The Tokyo metropolitan area is the most extensively urbanized region in Japan, and extensive sea breezes dominate this area during the afternoon on sunny summer days. On the other hand, a number of high-rise buildings are constructed in recent years due to using the limited urban area in high density, and it has been pointed out that this verticalization cause the interruption of sea breezes and the deterioration of the urban thermal environment.

Since the 1970s, inland penetration of sea breezes over the Kanto Plain in Japan has been investigated from a meteorological viewpoint (Kondo and Gambo, 1979; Fujibe and Asai, 1980). In those studies, air pollution was the main focus in environmental issues. From these results, it has been shown that the sea breeze is interrupted by an adverse pressure gradient due to lower pressure around the internal high temperature region (Gamo, 1988; Yoshikado and Kondo, 1989). Additionally, it is considered that the urban heat island is related to the

advance of the sea breeze (Kondo, 1990; Yoshikado, 1992; Kimura and Takahashi, 1991).

As for the city block scale, the interruption of sea breezes by tall buildings on the waterfront areas along Tokyo Bay has been studied previously (Masuda et al., 2005; Narita, 2006; Ashie, 2007). Against this background, strong winds blowing between tall buildings can be efficiently utilized to accelerate ventilation near the ground surface and to improve the urban environment in summer. Many of these studies focus on 2~3-km scale, whereas the effect of this utilization on a 100-km scale is not well understood. Moreover, assuming that the sea breeze is used to counter the urban heat island effect, it is likely that the energy in the sea breeze is used up and its potential travel distance changed.

In order to use sea breezes to counter the heat island phenomena, i.e. to improve urban ventilation efficiency, it is necessary to clarify the effect of building morphology on large-scale wind fields. In this study, the sea breeze in the vicinity of the Kanto Plain in Japan is simulated using a mesoscale meteorological model. Additionally, a mean kinetic energy balance model is proposed to estimate the structure of such sea breezes. The contribution ratio for diverse factors in the generation and inhibition of sea breezes is quantitatively demonstrated in terms of the mean kinetic energy balance.

[†]Corresponding author: Taiki Sato
Tel: +81-45-814-7239; Fax: +81-45-814-7256
E-mail: stutik00@pub.taisei.co.jp

2. Outline of Analyses

2.1. Outline of mean kinetic energy balance model

The authors have proposed a new concept “Thermal Energy Balance Model (TEBM)” (Ooka et al., 2011). In the model, an arbitrary domain in the urban area is regarded as the Control Volume (CV) to comprehensively calculate the thermal energy balance. The heat fluxes composing the thermal energy balance of the CV are calculated from numerical data provided by computational fluid dynamics (CFD) analyses of a mesoscale climate. Thus, the TEBM provides a means of analysing urban thermal environments, focused on thermal energy balance.

Here, as with the TEBM, the authors propose the mean kinetic energy balance model, in which the energy balance within a domain (Control Volume) moving along the sea breeze is evaluated. This model is composed of incoming and outgoing mean kinetic energy fluxes through all virtual surfaces of the CV, production, and dissipation in the CV as shown in Fig. 1. These energy fluxes are calculated from numerical data provided by CFD analyses based on mesoscale meteorological model.

In Fig. 1, Dissipation by resistance or urban canopy and Reynolds stress are affected by building complexes materially. Therefore, in order to represent the effects of building morphology, the mesoscale meteorological model used in this study is incorporating with the urban canopy model as the ground surface boundary condition (Ooka et al., 2011). Thus, a coupled simulation of horizontal advection of the flow field and resistance of building canopies is possible. Here, a uniform city block, i.e. a series of buildings with the same height (h_b), width (w_b), and interval (w_r), is assumed within each grid of CFD analysis as shown in Fig. 2. The shapes of the building

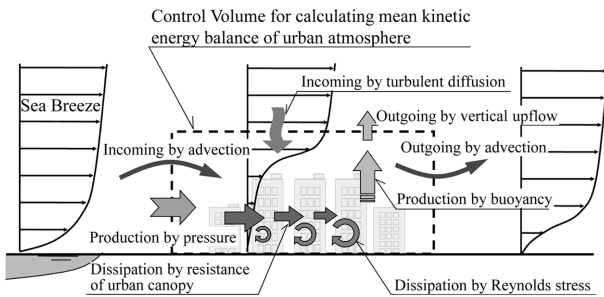


Figure 1. Concept of the mean kinetic energy balance model.

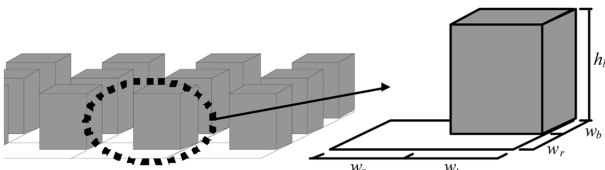


Figure 2. Modelling of building complex.

complexes of each grid are determined using a Digital Surface Model (DSM) and a Digital Elevation Model (DEM) prepared by an aeronautical laser profiler from three-dimensional geographical information system data (Setojima et al., 2002).

The equation of momentum is as follows:

$$\frac{\partial U_i}{\partial t} + \frac{\partial U_i U_j}{\partial x_j} + \frac{\varepsilon_{ijk} f_j U_k}{(c)} = -c_p \Theta \frac{\partial \pi}{\partial x_i} - \frac{g_i \beta \theta \delta_{i3}}{(e)} - \frac{\partial \overline{u_i u_j}}{\partial x_j} - \frac{\eta C_d a U_i \sqrt{U_i^2}}{(g)} \quad (1)$$

U_i : ensemble average velocities for x_i [m s^{-1}]

t : time [s]

x_i : coordiantes (x_1 : east-west direction, x_2 : north-south direction, x_3 : vertical direction) [m]

ε_{ijk} : permutation symbol

f_j : Coriolis parameter

c_p : specific heat of air at constant pressure [$\text{J kg}^{-1} \text{K}^{-1}$]

Θ : reference potential temperature [K]

π : difference between Exner function from a reference value [-]

g_i : gravity acceleration ($g_1 = g_2 = 0, g_3 = 9.8$) [m s^{-2}]

θ : difference between mean potential temperature and reference potential temperature [K]

β : thermal expansion coefficient ($= 1/\Theta$)

δ_{i3} : Kronecker delta

$\overline{u_i u_j}$: turbulent Reynolds stress (u_i : velocity fluctuations [m s^{-1}])

η : ratio of city block or planted area to the grid area [-]

C_d : drag coefficient (building canopy: 0.1, tree canopy: 0.2) [-]

a : the building or leaf area density [$\text{m}^2 \text{m}^{-3}$] ($= 4w_b/(w_r + w_b)^2$)

Each term of Eq. (1) means as follows: (a) Temporal derivation, (b) Advection, (c) Coriolis' force, (d) Production by pressure, (e) Production by buoyancy, (f) Turbulent diffusion by eddy viscosity, and (g) Dissipation by urban canopy resistance (buildings and tree canopies).

To multiply each term of Eq. (1) by U_i , the equation of mean kinetic energy is produced as shown in Eq. (2).

$$\frac{\partial E}{\partial t} + \frac{\partial E U_j}{\partial x_j} = -c_p \Theta \frac{\partial \pi U_i}{\partial x_i} - \frac{g_3 \beta \theta U_3}{(D)} + \frac{\overline{u_i u_j} \frac{\partial U_i}{\partial x_j}}{(E)} - \frac{\eta C_d a (U_i^2)^{\frac{3}{2}}}{(F)} + \frac{\partial (-\overline{u_i u_j} U_i)}{\partial x_j} \quad (2)$$

Here, E is the mean kinetic energy [$\text{m}^2 \text{s}^{-2}$]. Each term of Eq. (2) means as follows: (A) Temporal derivation, (B) Advection, (C) Production or dissipation by pressure gradient, (D) Production by buoyancy, (E) Dissipation by Reynolds stress, (F) Dissipation by urban canopy resist-

ance (buildings and tree canopies), and (G) Turbulent diffusion. By integrated at CV and applied to divergence theorem of Gauss, the mean kinetic energy balance of CV is derived as,

$$\begin{aligned} & \frac{\partial}{\partial t} \underbrace{\iiint_V E dV}_{(A')} + \underbrace{\iint_S E U_j n_j dS}_{(B')} = \\ & - \underbrace{\iint_S c_p \Theta \pi U_i n_i dS}_{(C')} - \underbrace{\iiint_V g_3 \beta \theta U_3 dV}_{(D')} + \underbrace{\iiint_V \overline{u_i u_j} \frac{\partial U_i}{\partial x_j} dV}_{(E')} \\ & - \underbrace{\iiint_V \eta C_d a (U_i^2)^{\frac{3}{2}} dV}_{(F')} + \underbrace{\iint_S (-\overline{u_i u_j}) U_i n_j dS}_{(G')} \end{aligned} \quad (3)$$

where V is volume of CV [m^3], S is surface area of CV [m^2], and n_j is component in the j direction of outward unit normal vector at the surface of CV. It is possible to evaluate the mechanism of the temporal variation of the energy by means of calculating the budget for the right side in Eq. (3). However, the calculation of the energy budget by a Lagrangian approach is required due to dealing with the moving CV along the sea breeze. Thus, Eq. (4) is used in this study.

$$\begin{aligned} & \frac{D}{Dt} \underbrace{\iiint_V E dV}_{(A)} = - \underbrace{\iint_S c_p \Theta \pi U_j n_j dS}_{(B)} - \underbrace{\iiint_V g_3 \beta \theta U_3 dV}_{(C)} \\ & + \underbrace{\iiint_V \overline{u_i u_j} \frac{\partial U_i}{\partial x_j} dV}_{(D)} - \underbrace{\iiint_V \eta C_d a (U_i^2)^{\frac{3}{2}} dV}_{(E)} + \underbrace{\iint_S (-\overline{u_i u_j}) U_i n_j dS}_{(F)} \\ & \frac{D}{Dt} \equiv \frac{\partial}{\partial t} + U_1 \frac{\partial}{\partial x_1} + U_2 \frac{\partial}{\partial x_2} + U_3 \frac{\partial}{\partial x_3} \end{aligned} \quad (4)$$

Here, U_i means the moving velocity of the moving CV.

2.2. Meteorological model

The meteorological model is based on a hydrostatic approximation. As a turbulence closure model, the Mellor-Yamada model (level 2.5) is used (Mellor and Yamada, 1974, 1982; Yamada and Bunker, 1989). The following factors relating to the building complex are incorporated into the mesoscale meteorological model: (1) wind reduction by the building complex, (2) production of turbulence by the building complex, (3) solar radiation heat transfer inside and outside of the building complex, (4) longwave radiation heat transfer inside and outside of the building complex, and (5) sensitive and latent heat transfer from the building surface. Four factors relating to the plant canopy are also incorporated into the mesoscale meteorological model, namely: (6) wind reduction by the plant canopy, (7) production of turbulence by the plant canopy, (8) solar radiation absorption by the plant canopy, and (9) transpiration from the plant canopy. These processes are explained by Ooka et al.(2011).

2.3. Computational domains and grid arrangements

The computational domains are shown in Fig. 3 and

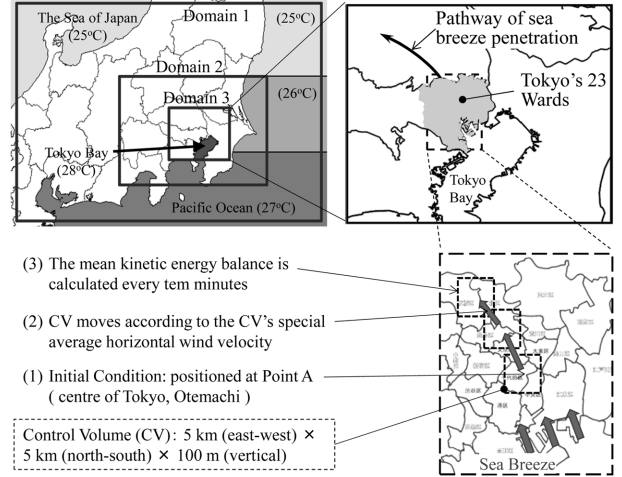


Figure 3. Computational domains and procedures to calculate mean kinetic energy of moving CV.

Table 1. Computational domains and grid arrangements

	Computational Domain x×y×z [km]	Grid Number	Horizontal Grid Size [km]
Domain 1	480×400×9.6	60×50×61	8
Domain 2	232×200×9.6	58×50×61	4
Domain 3	96×96×9.6	96×96×61	1

Table 1. In this study, sea breeze is focused on as one of the crucial environmental components. Because the sea breeze is formed by large-scale geographical conditions, the simulation is carried out using the one-way nesting method. The whole computational domain (Domain 1) is nested into two sub-domains: Domains 2 and 3. The coarse grid values at the boundaries of the nested area provide boundary conditions for the nested grid. Additional boundary values at the points between the coarse grids are obtained by liner interpolation. The vertical direction, z-axis, is divided from the ground surface up to an altitude of 9.6 km using 61 non-uniform meshes. Moreover, the subterranean layer from the ground surface to a depth of one metre is divided into 12 non-uniform meshes.

Fig. 3 also indicates the procedures to calculate the mean kinetic energy of the moving CV based on Eq. (4). The moving CV is positioned around Otemachi at 1200 JST. The domain is 5 km (north-south direction) × 5 km (east-west direction), and 100 m (vertical [Z] direction). The CV moves according to its special average horizontal wind velocity. The mean kinetic energy balance is calculated every ten minutes. In this paper, the results indicate the normalized value per unit volume based on the size of the CV.

2.4. Initial and boundary conditions

The initial conditions are shown in Table 2. The numerical experiments are carried out under a typical

Table 2. Initial and meteorological conditions

Initial potential temperature near the ground surface	26.0°C
Potential temperature gradient	5.0 K km ⁻¹ (0~5 km) 4.0 K km ⁻¹ (5~9.6 km)
Geostrophic wind (wind direction)	2.0 m s ⁻¹ (S)
Relative humidity near the surface	70%
Precipitable water	13 mm
Temperature at the sea surface (fixed)	Tokyo Bay: 28°C Pacific Ocean: 25~27°C The Sea of Japan: 25°C
Cloud cover ratio (fixed)	30%

summer meteorological situation. The simulations are started from 0600 JST(Japan Standard Time), and time integration is performed for 42 hours. The results obtained from 0000JST (18 hours after the calculation starts) to 2400JST (42 hours after the calculation starts) are used to evaluate the mean kinetic energy balance of the atmosphere.

The initial wind direction and velocity are set as southerly 2.0 m s⁻¹ at a height of 9.6 km from the ground surface across the entire computational domain. The large-scale entrance boundary values are fixed at the initial value, with the exit boundaries as free outflow. The boundary values for small domain are supplied by the large-scale results. Boundary conditions on the ground surface for transport equations of momentum, potential temperature, and specific humidity are provided based on the Monin-Obukhov similarity theory. At the top of the computational domain, the wind direction and velocity are fixed at the initial conditions. The details of the initial and boundary conditions are as given by Mochida et al. (1997).

In this study, the building energy consumption calculation is incorporated into the building canopy model in order to estimate the exhaust heat from air conditioning in the buildings. Usually, the air-conditioning heat load is composed of (1) the heat load through the walls, (2) the heat load through the windows, (3) the heat load due to ventilation, and (4) the heat load due to internal heat generation in the building. This air-conditioning heat load is released with the energy consumed by the air-conditioner from the air-conditioner's external unit. The transport equations in this study for potential temperature variation (air temperature) and mixing ratio of total water

(humidity) are incorporated in the artificial exhaust heat, air conditioning exhaust heat, sensible heat, and latent heat fluxes from building surfaces. The details are as given by Ooka et al. (2011).

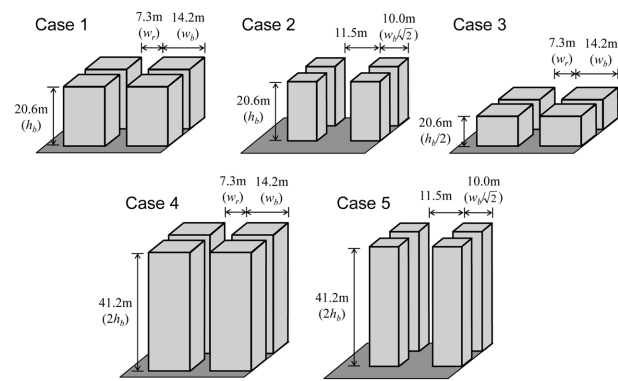
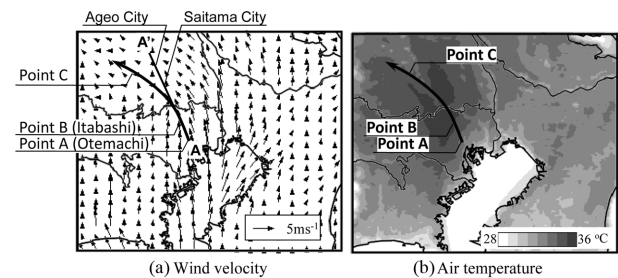
2.5. Computational cases

Five numerical experiments were carried out. Computed cases are summarized in Table 3 and Fig. 4. In Case 1, the present building morphology is incorporated into the prediction. In the other cases, the building height or building-to-land ratio is changed. Outside of Tokyo's 23 Wards, the height of all buildings (h_b) is 6 m and the width (w_b) is 7 m. The interval (w_r) is set based on the land-use ratio of building in each grid.

3. Numerical Analysis Results

3.1. Horizontal distributions of wind velocity and air temperature

Fig. 5 illustrates the horizontal distributions of the wind

**Figure 4.** Building morphology of each Case.**Figure 5.** Results of horizontal distributions (Case 1, Domain 3, 3 m height, 1200JST).**Table 3.** Analysis cases

Case no.	Building morphology in Tokyo's 23 Wards		
	Building height	Building-to-land ratio	Floor-area ratio
1	Present status	Present status	Present status
2	Present status	Half size of Case 1	Half size of Case 1
3	Half size of Case 1	Present status	Half size of Case 1
4	Double size of Case 1	Present status	Double size of Case 1
5	Double size of Case 1	Half size of Case 1	Present status

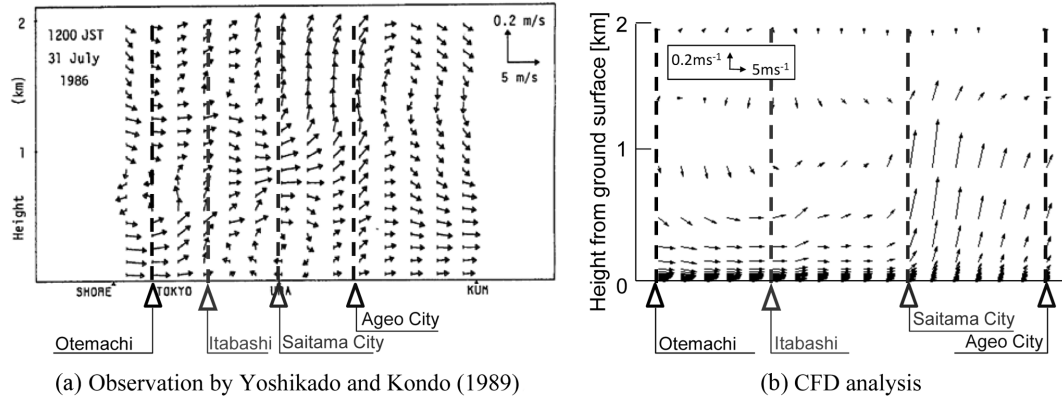


Figure 6. Comparison of vertical distribution of wind velocity (1200JST, A-A' section).

velocity and air temperature at a height of 3 m at 1200 JST. As more wind passes from the bay side towards the inland area of the Kanto Plain, the wind becomes weaker. The flow pattern of sea breezes in the afternoon is consistent with a number of observations. The high temperature area spreads from around the north side of the centre of Tokyo to the leeward side.

3.2. Comparison of flow field between CFD results and observation data

Fig. 6 shows wind velocity in the vertical cross-section along A-A' in Fig. 5(a) at 1200JST. Fig. 6(a) is the observation data from Yoshikado and Kondo (1989), and Fig. 6(b) is the calculated results. The calculation agrees with the observation as follows. The sea breeze is detected as a strong wind near the ground surface from Otemachi to Itabashi, and an upward flow around Itabashi at the leading edge of the sea breeze is identified. This upward flow suggests that the leading edge may slide over the calm inland atmosphere. Moreover, another strong upward flow due to high temperature is found above the weak wind area from Saitama City to Ageo City.

Fig. 7 explains the comparison of the temporal variations for the horizontal wind velocities around each city. The vertical axis is the distance north-westward from A to A', while the arrows indicating wind vectors are drawn in such a way that an upward one corresponds to a northward wind. The area of "S" in Fig. 7(a), which has been hatched by the authors, represents the sea breeze developing area. The onset of the sea breeze at Otemachi occurred about 1000JST a.m., and then heads inland with time. The arrival time of the front edge of the sea breeze based on these calculations is fairly consistent with observation data.

3.3. Temporal variation in moving velocity and temperature of CV

The temporal variations in the moving velocity and temperature of the moving CV are shown in Fig. 8. The moves of CV is explained Sect. 2.3. Penetration pathways

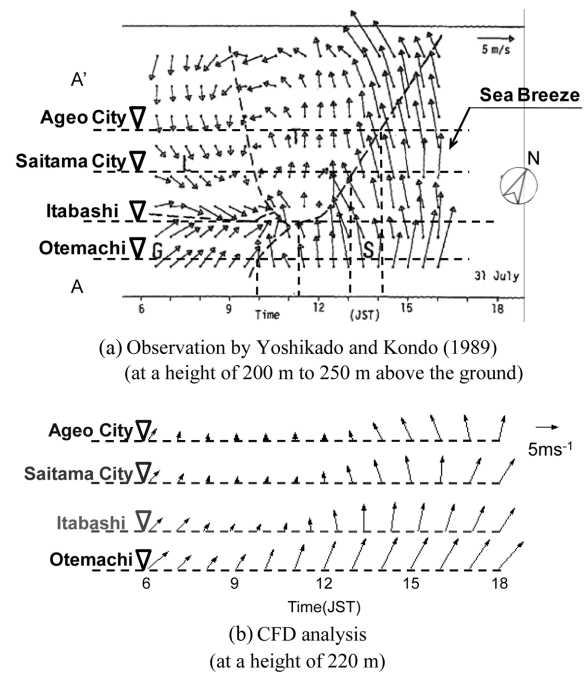


Figure 7. Comparison of arrival time of sea breeze.

in Case 2-5 are roughly equivalent to Case 1. However, the arrival time for each city is different. In this paper, Cases 1, 3, and 4 are focused on.

The moving velocity in Case 1 is indicated as about 5.5 m s^{-1} at 1200JST (i.e. Point A). The value reaches a maximum at about Point B, and decreases to 2.5 m s^{-1} after passing Point B. In Case 3, the moving velocity is about 1.0 m s^{-1} higher than that in Case 1 from Point A to Point B, and that in Case 4 is about 2 m s^{-1} lower than that in Case 1 after passing Point B.

The temperature of the moving CV in each case considerably increases from Point A to Point B. The temperature in Case 3 is slightly higher than in Case 1. This appears to be caused by an increase in the ground surface temperature due to increased incident short-wave radiation on the ground surface. In contrast, verticalization in Case 4 reduces the air temperature. This result

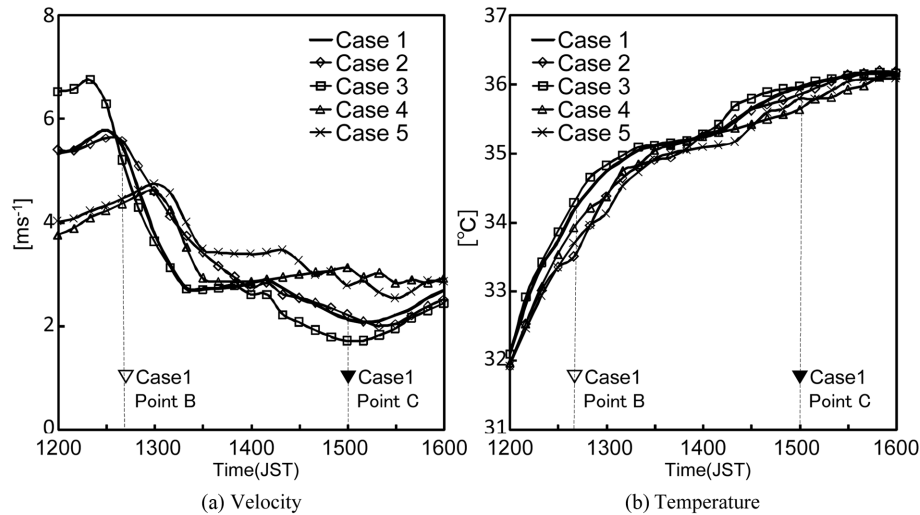


Figure 8. Temporal variation of velocity of moving CV.

is caused by a decrease in the radiation at the ground surface, and the effect continues inland.

4. The Mean Kinetic Energy Balance of Moving CV

Figs. 9 and 10 present the calculated results based on the mean kinetic energy balance model. In these figures, positive signs in the vertical axis indicate a mean kinetic energy incoming on the virtual surface of the CV or production within the CV. On the other hand, negative signs indicate an outgoing from the surface of the CV or dissipation within the CV. Fig. 9 shows the mean kinetic energy balance of the moving CV along the sea breeze penetration from Point A to C (cf. Fig. 1). Here, Cases 1, 3, and 4 are especially considered as in the case in Sect 3.3.

In Case 1, the pressure gradient term (\diamond) is positive (i.e. favorable pressure gradient) from Point A to Point B (in Tokyo's 23 Wards). It can be seen that this causes an increase in the mean kinetic energy of the sea breeze. At the same time, the resistance of the urban canopy (\blacklozenge) and the friction of the ground surface and Reynolds stress (\bullet) due to the velocity gradient are negative. This means that these terms are interruptive factors for the sea breeze. This is believed to be caused by its passing through the urban area at a relatively high velocity. These terms are negative from about 1250JST until about 1320JST after passing Point B. Additionally, no favorable pressure gradient is observed. As a result, the total budget of the mean kinetic energy for the CV drops to a negative value. This is the reason that the moving velocity significantly decreases during this period. Against these interruptive factors, the mean kinetic energy is supplied from the upper side of the CV by turbulent diffusion (\blacktriangle). As for buoyancy term (\times), the value indicates positive value after passing Point B. Conversely, the

pressure gradient term drops to a negative value (i.e. adverse pressure gradient). The former is caused by warmer air near the ground surface. The latter is caused by the lower pressure due to raised temperatures. This causes dissipation of the mean kinetic energy, and decreases the wind velocity (cf. Fig. 8(a)). Therefore, the pressure gradient becomes an interruptive factor for the sea breeze once it reaches inland areas. This result from the viewpoint of mean kinetic energy is indicative of an interruptive factor pointed out by previous research.

In Case 3, the favorable pressure gradient from Point A to B is larger than that in Case 1. The reason is assumed to be that the temperature of the CV in Case 3 is larger than Case 1 (cf. Fig. 8(b)). Additionally, dissipation due to resistance by the urban canopy and the Reynolds stress is less with the reduction in building height. These contribute to the retention of its velocity. On the other hand, the adverse pressure gradient increases with the increase in temperature in the inland region. Finally, the velocity is the lowest of the five cases (c.f. Fig 8(b)).

In Case 4, with the decrease in the CV's temperature, the favorable pressure gradient is lowered. In addition, the resistance from buildings causes an increase in the dissipation of mean kinetic energy. As a result, the velocity of the moving CV is lower than that in Case 1 from Point A to B (i.e. the centre of Tokyo). In contrast, in terms of the temperature decrease, the adverse gradient pressure is lower than those in the other cases. Therefore, the moving velocity of the CV does not decrease after passing Point B. As a result, the CV of Case4 has the largest value of the moving velocity around Point C (cf. Fig. 8(a)).

Here, to factor out the effect of changes in the mean kinetic energy itself, the values in Fig. 8 are normalized by dividing by the mean kinetic energy value for each instant in time as shown in Fig. 10. By this process, the characteristics of each case become more remarkable.

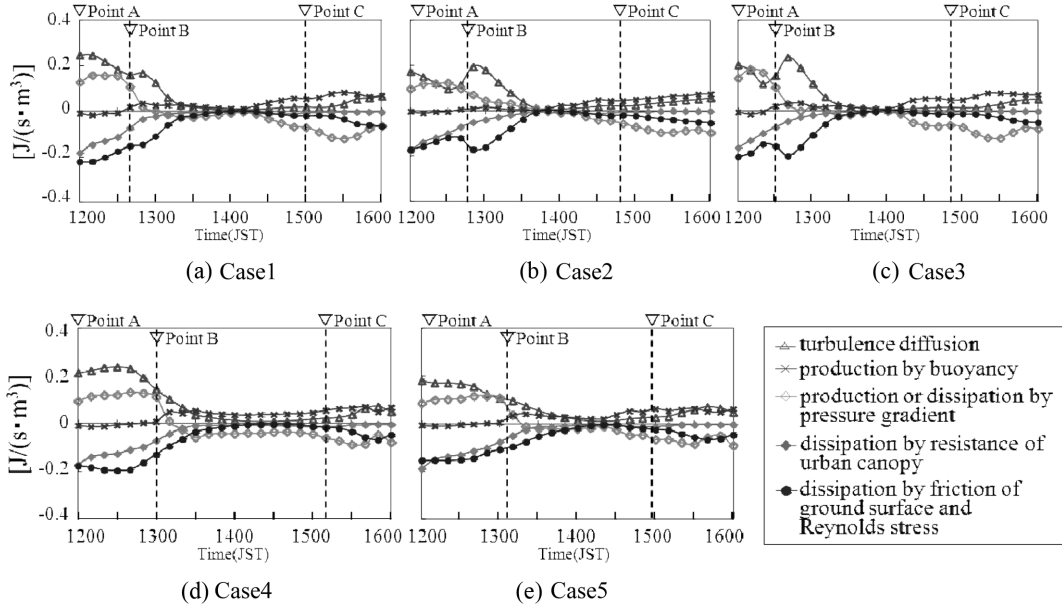


Figure 9. Temporal variation of the mean kinetic energy balance of the moving CV along the sea breeze penetration.

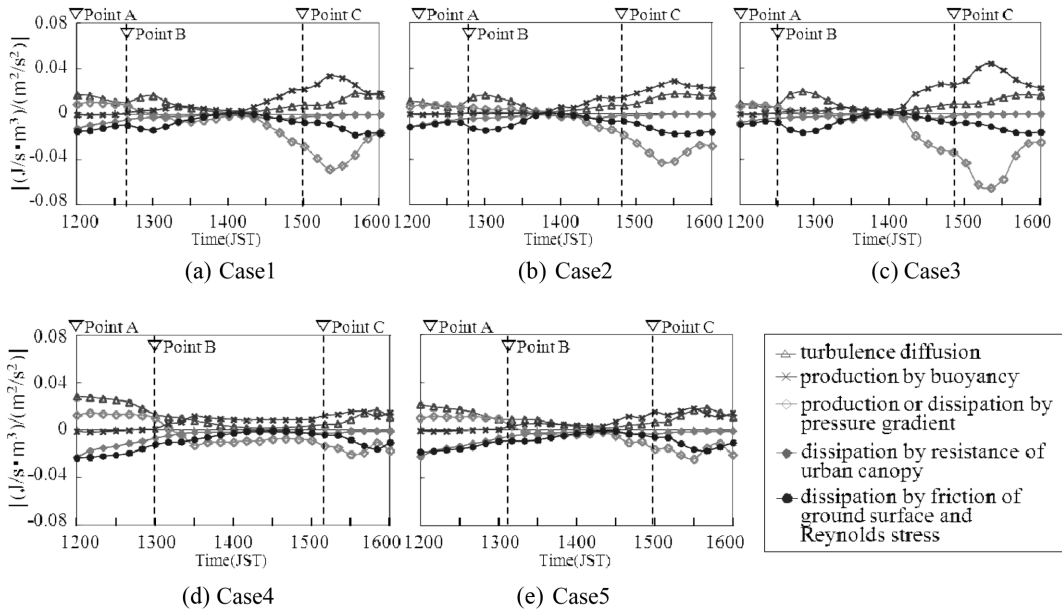


Figure 10. Temporal variation of the normalized values in Figure 8 by the value of the mean kinetic energy for each instant in time.

The dissipation by resistance from the urban canopy in Case 3 is lower than that in Case 1 from Points A to B (i.e. the centre of Tokyo). On the other hand, that in Case 4 is larger than that in Case 1. In other words, it seems that using strong winds blowing through tall buildings as a countermeasure to promote urban ventilation decreases the mean kinetic energy of the sea breeze near the ground surface. Moreover, this leads to acceleration in the transport of mean kinetic energy from the upper layer to the lower boundary layer. Finally, it is likely that the behaviour of the sea breeze and the penetration area are

changed, not only around the bay area, but also the inland area.

5. Conclusions

- (1) The sea breeze around the Kanto Plain in Japan is simulated using a mesoscale meteorological model incorporating the urban canopy model. The characteristic of flow fields based on the numerical simulation agree well fairly consistent with that from observation data.

- (2) The mean kinetic energy balance model is proposed to estimate the structure of the sea breeze. In the model, the contribution ratio of diverse factors for sea breeze generation and inhibition is quantitatively demonstrated in terms of the mean kinetic energy balance.
- (3) In the centre of Tokyo, a favorable pressure gradient causes an increase in the mean kinetic energy of the sea breeze. At the same time, the resistance from the urban canopy and the Reynolds stress due to the velocity gradient interrupt the sea breeze. This inhibition of the mean kinetic energy of the sea breeze leads to provision of the energy from the upper atmosphere by turbulent diffusion. Inland, the mean kinetic energy is generated by buoyancy and the dissipated adverse pressure gradient becomes the interruptive factor for the sea breeze.
- (4) Assuming a building height half that of the present, dissipation by resistance from the urban canopy and the Reynolds stress decreases. Moreover, the temperature of urban area becomes higher than present, the wind velocity increases around the bay area due to an increase in the favorable pressure gradient around the bay area. On the other hand, the wind velocity inland decreases with an increase in an adverse pressure gradient inland.
- (5) Assuming a building height double that of the present, the opposite results in case of reducing the building height to half are shown. The dissipation by resistance from the urban canopy and the Reynolds stress increases, and the temperature becomes lower than present. As results, the wind velocity decreases around the bay area, while that inland increases from the weakness of the adverse pressure gradient.

References

- Ashie, Y. (2007) "Numerical Simulation of Urban Thermal Environment in the Waterfront Area of Tokyo", Annual Report of the Earth Simulator Center, April 2005 - March 2006, pp. 83-87.
- Fujibe, F. and Asai, T. (1980) "Some features of a surface wind system associated with the Tokyo heat island", *Journal of Meteorological Society of Japan*, 58, pp. 149-152.
- Gamo, M. (1988) "Hourly Change of Advance of the Sea-breeze Front over Kanto Area", *Kogai*, 23, pp. 37-46 (in Japanese with English abstract).
- Inter-Ministry Coordination Committee to Mitigate Urban Heat Island (2004) "Outline of the Policy Framework to Reduce Urban Heat Island Effects".
- Kimura, F. and Takahashi, S. (1991) "The effects of land-use and anthropogenic heating on the surface temperature in the Tokyo metropolitan area: A numerical experiment", *Atmospheric Environment*, Part B, 25B (2), pp. 155-164.
- Kondo, H. and Gambo, K. (1979) "The effect of the mixing layer on the sea breeze circulation and the diffusion of pollutants associated with land-sea breeze", *Journal of Meteorological Society of Japan*, 57, pp. 560-575.
- Kondo, H. (1990) "A numerical experiment of the extended sea breeze over the Kanto Plain", *Journal of Meteorological Society of Japan*, 68(4), pp. 419-434.
- Masuda, Y. et al. (2005) "A Basic Study on Utilization of the Cooling Effect of Sea Breeze in Waterfront Areas along Tokyo Bay", *Journal of Asian Architecture and Building Engineering*, 4(2), pp. 483-487.
- Mellor, G. L. and Yamada, T. (1974) "A Hierarchy of Turbulence Closure Models for Planetary Boundary Layer", *Journal of Applied Meteorology*, 13(7), pp. 1791-1806.
- Mellor, G. L. and Yamada, T. (1982) "Development of a Turbulence Closure Model for Geophysical Fluid Problem", *Rev. Geophys. Space Phys.*, 20(4), pp. 851-875.
- Mochida, A. et al. (1997) "CFD analysis of mesoscale climate in the Greater Tokyo area", *Journal of Wind Engineering and Industrial Aerodynamics*, 67-68, pp. 459-477.
- Narita, K. (2006) "Wind Tunnel Experiments on the Effects of High-rise Buildings on the Wind Field in Shiodome Area", *Journal of Architecture and Building Science*, 24, pp. 237-240 (in Japanese with English abstract).
- Ooka, R. et al. (2011) "Thermal Energy Balance Analysis of the Tokyo Metropolitan Area Using a Mesoscale Meteorological Model Incorporating an Urban Canopy Model", *Boundary-Layer Meteorology*, 138, pp. 77-97.
- Setojima, M. et al. (2002) "Measurement of Forest Area by Airborne Laser Scanner and Its Applicability", *Journal of Japan Society of Photogrammetry and Remote Sensing*, 41(2), pp. 15-26 (in Japanese).
- Taha, H. (1997) "Urban Climates and Heat Islands: Albedo, Evapotranspiration, and Anthropogenic Heat", *Energy and Buildings*, 25, pp. 99-103.
- Yamada, T. and Bunker, S. (1989) "A Numerical Model Study of Nocturnal Drainage Flows with Strong Wind and Temperature Gradients", *Journal of Applied Meteorology*, 28, pp. 545-554.
- Yoshikado, H. and Kondo, H. (1989) "Inland Penetration of the Sea Breeze over the Suburban Area of Tokyo", *Boundary-Layer Meteorology*, 48(4), pp. 389-407.
- Yoshikado, H. (1992) "Numerical Study of the Daytime Urban Effect and Its Interaction with the Sea Breeze", *Journal of Applied Meteorology*, 31(10), pp. 1146-1164.